The Shrinking Fermi Liquid Scenario for Cuprates Under the Scrutiny of Optical Conductivity Measurements

Sergio Caprara , Carlo Di Castro , Giovanni Mirarchi , Götz Seibold , Marco Grilli *

Posted Date: 21 October 2024

doi: 10.20944/preprints202410.1519.v1

Keywords: strange metal; cuprates; optical conductivity; Shrinking Fermi liquid

 doi:10.20944/preprints202410.1519.v1

Article

The Shrinking Fermi Liquid Scenario for Cuprates under the Scrutiny of Optical Conductivity Measurements

Sergio Caprara [1], Carlo Di Castro [1], Giovanni Mirarchi [1,2], Götz Seibold [3] and Marco Grilli [1,*]

[1] CNR-ISC, and Dipartimento di Fisica, Università di Roma Sapienza, Piazzale Aldo Moro 5, 00185 Roma, Italy
[2] Institut für Theoretische Physik und Astrophysik, Universität Würzburg, Am Hubland, 97074 Würzburg, Germany
[3] Institut für Physik, Brandenburg Technical University Cottbus-Senftenberg, D-03013 Cottbus, Germany
* Correspondence: marco.grilli@roma1.infn.it

Abstract: In a recent paper [B. Michon et al., Nat. Commun. (2023) 14:3033] optical conductivity experiments in cuprate superconductors were shown to display scaling properties consistent with the Marginal Fermi Liquid theory. Here we argue, that the temperature regime studied in these experiments does not allow to distinguish between Marginal Fermi Liquid and a Shrinking Fermi Liquid. In the latter scenario, which we recently proposed and which applies near a quantum critical point, dynamical fluctuations of the order parameter with short correlation length mediate a nearly isotropic scattering among the quasiparticles over the entire Fermi surface leading to strange-metal behavior. If the damping of these nearly local fluctuations increases by decreasing the temperature, the Fermi liquid regime shrinks and the strange-metal behavior is extended to the lowest temperatures. This Shrinking Fermi liquid scenario has many similarities and some differences with respect to the Marginal Fermi liquid theory. In particular, we show that the approximate scaling properties of the optical conductivity in some high-frequency regime predicted by the Shrinking Fermi liquid scenario account to a very good extend for the experimental data.

Keywords: strange metal; cuprates; optical conductivity; shrinked Fermi liquid

1. Introduction

1.1. The General Framework: Strange Metallicity in Cuprates and Elsewhere

The anomalous properties of superconducting cuprates in their metallic state has always raised the issue of a new state of matter requiring a revision of the paradigmatic Landau Fermi liquid theory valid for ordinary metals. The occurrence of this 'Strange Metal' state, see e.g. Ref. [1,2], is a major theoretical and experimental challenge also because it occurs in many other systems like heavy fermions, pnictide superconductors, twisted bilayer graphene, and so on. At the moment the main theoretical trends in this regard involve the coupling of the fermionic quasiparticles with low-energy nearly local dynamical bosonic degrees of freedom. Recently, it has been proposed to represent these excitations by a so-called Sachdev-Ye-Kitaev model [3–5]. Similar results are obtained in Ref. [6], where the itinerant fermions are coupled to a two-level system. These bosonic excitations might arise from some small-momentum order parameter fluctuations (e.g., nematic) near a quantum critical point (QCP). Disorder is then responsible for turning these long-ranged excitations into local excitations.

On the other hand, the recent discovery [7,8] of nearly local charge density fluctuations (CDF) in the form of 'aborted', very short ranged, charge density waves (CDW) has triggered the idea that CDF are the sought nearly local degrees of freedom [9]. Assuming that the damping of CDF may increase when superconductivity is suppressed (usually by strong magnetic fields) the characteristic energy of CDF ω_0^{CDF} decreases thereby extending the strange metal behavior down to lower temperatures. This is the so-called Shrinking Fermi Liquid scenario [10–12], see Section 1.2. In this framework, in order to understand the strange metal state it is of primary relevance to extract from experiments indications on the low-energy dynamical excitations.

 doi:10.20944/preprints202410.1519.v1

Concerning the dynamical aspects of the strange-metal phase the associated dynamical scattering rate can in principle be extracted from optical conductivity data. Motivated by possible quantum critical behavior, a number of experiments have been devoted to an analysis of the frequency dependent scaling behavior [13–16], where early experiments [17,18] provided evidence for a power-law behavior $\sigma(\omega) \sim 1/(\mathrm{i}\omega)^{\alpha}$, with a material and doping dependent exponent $\alpha < 1$. More recently, it has been shown that such an apparent power-law behavior is in fact compatible with an underlying (local) self-energy which obeys ω/T scaling [16]. In particular, it has been claimed that a Marginal Fermi Liquid (MFL) structure [19] $\mathrm{Im}\,\Sigma(\omega) \sim \beta\hbar\omega \coth(\beta\hbar\omega)$, with $\beta \equiv (kT)^{-1}$, can account for the optical conductivity data in $La_{2-p}Sr_pCuO_4$ (LSCO) at doping $p = 0.24$, when both $\hbar\omega$ and kT are below a high-energy cutoff $\sim 0.2\,\mathrm{eV}$. Moreover, the extracted seemingly logarithmic divergence of the optical mass upon reducing temperature is then taken as an additional support for the analysis, since on the one hand this is compatible with the expected mass renormalization of fermions in a MFL state and on the other hand is consistent with the observed logarithmic enhancement of the specific heat in LSCO for the same doping value [20]. However, these conclusions are drawn from an analysis of optical conductivity data for temperatures $T \gtrsim 40\,\mathrm{K}$ so that the logarithmic divergence of the optical mass for $T \to 0$ is somewhat ambiguous. Furthermore, optical measurements are affected by a bunch of excitations living in the optical frequency range, that can overshadow the contribution of the low-lying excitation that rule the DC transport.

In this paper, we will demonstrate that the Shrinking Fermi Liquid (SFL) theory [10–12] provides an alternative, and in some aspects more consistent, scenario in order to describe the optical conductivity data of cuprates. This theory is based on the coupling of charge carriers to CDF, as discussed above, and is characterized by an additional energy scale ω_{FL} which separates Fermi Liquid (FL) (for $\omega < \omega_{FL}$) from non-FL (for $\omega > \omega_{FL}$) behavior. Since in some doping ranges neither too far nor too close to the CDW quantum critical point (usually hidden in the superconducting region near optimal doping) ω_{FL} can become small at low temperatures [10,11] , the scenario was termed SFL. Here, we will argue that the violation of the MFL paradigm in the optical conductivity below $\beta\hbar\omega \sim 20$ [16] is fully compatible with an underlying FL state with $\omega_{FL} \approx 5 - 10\,\mathrm{meV}$ comparable with the characteristic energy of CDF ω_{CDF} [8]. In this regime, therefore, it is even not necessary to assume that this scale shrinks below the characteristic values observed for CDF, as it is instead required to account for the linear-in-temperature resistivity and logarithmic specific heat, because these phenomena occur instead when superconductivity is suppressed down to a few Kelvin. Nevertheless this (not necessarily shrunk) FL state accounts for the temperature dependent mass renormalization observed in optical experiments.

The paper is organized as follows: In the next Section 1.2 we recapitulate the main features of the SFL theory based on the exchange of CDF. In the subsequent Section 2 the evaluation of the optical conductivity within the SFL theory is undertaken. First, in Section 2.1, we discuss the energy spectra of CDF as probed by RIXS, which, together with the phonon, paramagnon, and particle-hole contribution, constitute the dominant low-energy excitations in a large class of cuprate materials. Then, in Section 2.2, we report our calculations of optical conductivity within the SFL scenario and in Section 3 we conclude our discussion.

1.2. The Shrinking Fermi Liquid Scenario

The last decade was characterized by an impressive progress in Resonant Inelastic X-ray Scattering (RIXS), which unambiguously confirmed [21–23] that a strong tendency to form CDW is present in underdoped and optimally doped cuprates, as predicted long ago [24–28]. More recently, RIXS experiments observed short-range dynamical CDF, pervading most of the cuprates phase diagram [7,8]. These fluctuations have nearly the same periodicity of the CDW, but, while they coexist in the underdoped region below the pseudogap crossover temperature T^*, CDF alone are found up to the highest temperatures and dopings. In comparison to CDW, the CDF have a substantially shorter coherence length and a higher (but still rather small) characteristic energy $\omega_0^{CDF} \sim 8 - 25\,\mathrm{meV}$ vs.

 doi:10.20944/preprints202410.1519.v1

$\omega^{CDW} \sim 0-3\,\mathrm{meV}$. Roughly speaking, owing to this distinct dynamical behavior, one can think of the CDF as 'aborted' CDW, which are nonetheless more robust both in temperature and doping, and indeed they have been detected over very broad parameter ranges and essentially in all classes of cuprates [29]. Remarkably, the abundant CDF are the only excitations that are detected at relatively low energy in the optimal and overdoped regions at temperatures above T_c. Therefore they are a natural candidate to explain the strange metal properties [1,3,4,30–35], most prominently the linear-in-temperature resistivity [36–38], in the metallic state of cuprates [9–12].

The main idea is that the CDF fulfill two rather general sufficient conditions to obtain linear-in-temperature resistivity: (a) they are sufficiently short ranged (i.e., nearly local in space) to provide a broad range of momenta in the scattering processes of quasiparticles. This first condition is needed in order to have the quasiparticles scattered all over the Fermi surface, thereby bypassing the objection of Ref. [39], which applies whenever the scattering is peaked at finite momenta, resulting in a partition of the Fermi surface in strongly scattered (hot) regions and weakly scattered (cold) regions. (b) the CDF have sufficiently low energy to obey a semiclassical statistical distribution down to T_c; Owing to this latter condition, the Bose distribution of the collective scatterers is well approximated by T/ω, resulting in a corresponding scaling behavior of the self-energy and, for $\omega = 0$, to a linear-in-temperature scattering rate, which is then responsible for the linear-in-temperature resistivity.

Our starting point is that the observed (and experimentally characterized) CDF have a propagator of the typical form for fluctuations around Gaussian QCP [40], in the presence of Landau damping $\sim \gamma$

$$D(\mathbf{q},\omega) = \frac{1}{M + \nu|\mathbf{q}-\mathbf{Q}_c|^2 - \frac{\omega^2}{\bar{\Omega}} - \mathrm{i}\gamma\omega}\,. \tag{1}$$

Here, M and ν represent energy and stiffness of the CDF, whereas $\bar{\Omega}$ is a crossover scale above which CDF acquire a more propagating character.

Previous work [9] has shown that CDF alone with $\gamma \sim 1$ can well account for the anomalous MFL-like properties of cuprates. In particular, these fluctuations have a quite short ranged character and therefore have weak momentum dependence, thus fulfilling the condition (b) mentioned above. At the same time, the characteristic energy can be as low as 8 meV [8] and can therefore fulfill also the condition (a) to give a linear-in-temperature inelastic quasiparticle scattering down to temperatures of order T_c. Also the electron self-energy up to frequencies of order $0.15-0.2\,\mathrm{eV}$ was well described by the coupling with CDF.

One major limitation of the above theory is that, by lowering the temperature, FL properties are recovered (i.e., the usual T^2 and ω^2 behavior of the imaginary part of the fermion self-energy) below a temperature slightly smaller than the FL scale $\omega_{FL} = M/\gamma$, which is of order $40-60\,\mathrm{K}$, at least. This is at odds with the observation of linear-in-temperature resistivity down to much lower temperature, when superconductivity is suppressed by strong magnetic fields [41]. The condition (b) above prevents to lower ω_{FL} by decreasing $M \sim \xi^{-2}$ approaching the QCP, because this would increase ξ (critical slowing down) and lead to strongly peaked momentum dependence of the fluctuation propagator. An alternative was recently proposed [10] to decrease the FL scale M/γ: assuming a temperature dependent dissipation parameter $\gamma \sim \log(1/T)$ the FL scale decreases *without* producing an increase of the spatial correlations (i.e., a reduction of M). The specific logarithmic form of $\gamma(T)$ was phenomenologically inferred from the logarithmic increase of the low-temperature specific heat coefficient C_V/T under strong magnetic field [42]. In this case, the boson contribution to C_V acquires a logarithmic contribution $C_V \sim T\gamma(T)\log(1/M)$. While the standard QCPs may display a logarithmic temperature dependence from a vanishing mass of the fluctuations $M \sim \xi^{-2} \sim T$, here the system is assumed to be close, but not too much, to the QCP in order to have abundant fluctuations at finite (actually, rather small) correlation length and mass M. Then, the observed logarithmic behavior stems from dissipation of the fluctuations $\gamma(T)$ and is neither due to the standard critical behavior of the fluctuations nor to the diverging fermion quasiparticle mass m^*, as found instead in the MFL theory.

 doi:10.20944/preprints202410.1519.v1

This scenario has been extended along two directions. In Ref. [11], a simple model where the low-energy CDF not only can decay in particle-hole pairs, but also into slow diffusive modes that always occur even in rather clean Drude metals whenever T is lower than the elastic scattering rate $1/\tau$. In two dimensions, this additional decay channel was shown to give rise to a logarithmic increase of the damping term γ. Of course, this is just one out of several other possibilities leading to an increasing damping, and further general effective mechanisms are still under investigation. On the other hand, a simplified fully local model of overdamped dispersionless Holstein phonons (ODHP) was recently investigated [12] in order to gain an analytical understanding of the scattering rate and self-energy of a FL in the case of a temperature-dependent scale $M/\gamma(T)$. The frequency and temperature dependence of the quasiparticle self-energy was shown to be almost indistinguishable from what expected for a MFL. Despite these strong similarities between our SFL scenario and the MFL scenario, some crucial differences are present. First of all, while it is well known that the quasiparticle mass m^* diverges logarithmically in T within the MFL scheme, in the SFL the quasiparticle mass is increased by the scattering with ODHP, but it always stays finite. Another major difference is that in MFL the dynamical quantities like electron self-energy and conductivity display a ω/T scaling, while such property is absent in the SFL case. This is not surprising, because the linear-in-temperature behavior of the scattering rate in SFL merely arises from the semiclassical statistical distribution function of the CDF while the frequency dependence is related to the spectral features of the excitations. Then an effective scaling is only obtained when $M/\gamma \to 0$ or for $\omega, T \gg M/\gamma$.

2. Optical Conductivity within the SFL Scenario

The above summary of the SFL scenario indicates that CDF alone can consistently account for the low-energy (thermodynamic and transport) properties of the metallic state of cuprates. The question naturally arises whether the SFL can also account for other spectroscopic properties of cuprates. In particular, it was recently shown [16] that optical experiments are in good agreement with MFL theory and, owing to the similarities between MFL and SFL, this latter may provide an equally good explanation for optical data.

2.1. The Experimental Characterization for Charge Density Fluctuations

The CDF represented by Equation (1) have a spectral density as shown by the red curve in Figure 1 and provide the microscopic basis for the theory at low energies. On the other hand, more standard, excitations (phonons, particle-hole and paramagnon excitations) are phenomenologically encoded as an additional flat contribution extending up to several fractions of eV. This is represented by the blue curve in Figure 1. Obviously, to describe the spectroscopic properties of cuprates at higher frequencies in optical experiments, one cannot neglect the whole set of excitations that are experimentally detected at higher energies (say from $0.05 - 0.5\,\mathrm{eV}$). Thus, besides the CDF spectral density, we also consider the non-CDF excitations (namely phonons, particle-hole and paramagnon excitations) as seen in the experimental RIXS spectral density of Figure 1c of Ref. [8]. Besides their rather low characteristic energy scale ω_0^{CDF}, CDF are characterized by a structure factor which is broad in momentum and in frequency. The spectra, as a function of momenta, display a broad maximum centered at a $\mathbf{Q}_c$, rather close to the CDW critical vector (indicating that these charge excitations mostly differ by their correlation length only). This peak is so broad (i.e., the associated spatial correlations are so short) that, as far as its effect on charge carriers is concerned, it can well be approximated by a constant as for a fully local overdamped excitation and be represented by an ODHP [12]. A remarkably flat RIXS spectrum is also observed as a function of frequency for $\mathbf{q} = \mathbf{Q}_c$. The frequency dependent RIXS spectra have then be fitted by several gaussian contributions: slightly above the elastic peak (due to disorder in the surface, static deformation and charge inhomogeneities) the CDF give rise to a contribution from 8 to $30 - 50\,\mathrm{meV}$. Excitations at higher energies are instead due to phonons, particle-hole and paramagnon excitations, etc. Here, we employ a minimal model for such a multi-excitation RIXS spectrum by restricting to the CDF and an effective higher energy contribution, cf.

 doi:10.20944/preprints202410.1519.v1

Figure 1, mimicking the experimental spectrum in Figure 1c of Ref. [8]. Notice also that, although the higher energy excitations have a composite nature, for the sake of brevity, we nickname as due to 'paramagnon' the whole flattish blue curve of Figure 1.

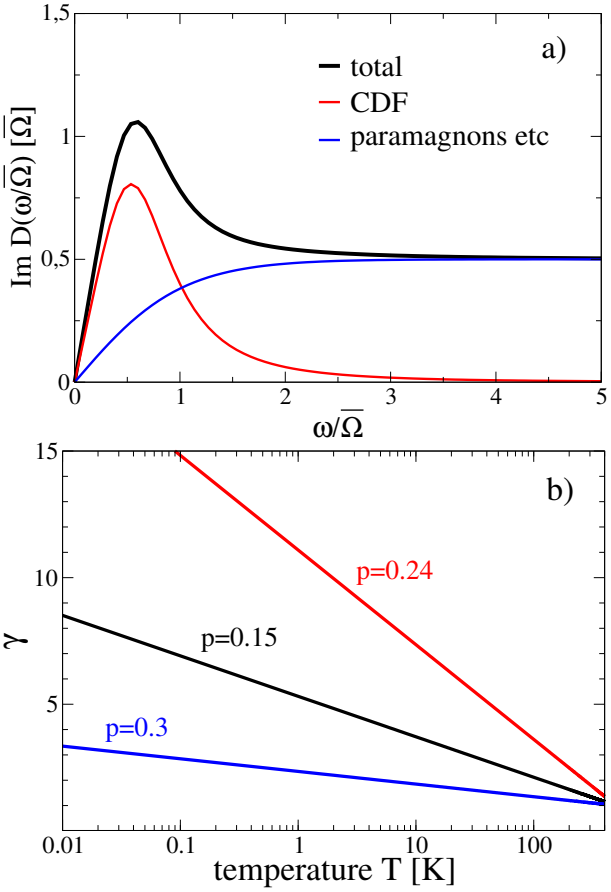

Figure 1. (a) The total spectral density [black, Equation (2)] is composed of the CDF (red) and an effective higher energy contribution (blue) which encompasses phonons, particle-hole and paramagnon excitations Parameters: $\alpha = 0.5$, $\omega_p/\bar{\Omega} = 1$, $m/\bar{\Omega} = 0.6$, $\gamma = 1.83$ is evaluated from Equation (3) for $T = 300\,\mathrm{K}$ and doping $p = 0.24$. (b) Temperature dependence of the γ parameter from Equation (3) for doping $p = 0.15$ (black), $p = 0.24$ (red), $p = 0.3$ (blue) and further parameters are specified in the text.

Therefore, we carried out the theoretical calculation of the cuprate optical properties by assuming the combined contribution of CDF, schematized as an ODHP (red line in Figure 1), and of additional non-CDF excitations, represented by the blue line in Figure 1.

The total spectral density of these excitations reads (We set henceforth $\hbar = 1$):

$$D_2(\omega) \equiv \mathrm{Im}\, D(\omega) = \frac{\gamma\omega}{(m - \omega^2/\bar{\Omega})^2 + \gamma^2\omega^2} + \frac{\alpha}{\bar{\Omega}} \tanh(\omega/\omega_p), \tag{2}$$

where the first term corresponds to the CDF, Equation (1), with the modification that, due to the broadness of the peak, the momentum dependence is neglected and the resulting purely local CDF are characterized by an effective mass m. For the temperature dependent damping parameter γ, cf. Section 1.2, we adopt the phenomenological form of Ref. [11]

$$\gamma = \gamma_0 + A(p)\log\left[\max\left(\frac{1}{\tau T}, 1\right)\right], \tag{3}$$

 doi:10.20944/preprints202410.1519.v1

with a doping dependent prefactor $A(p)$ specified in Equation (7) of Ref. [11]. Here, we focus mainly on the optical data from Ref. [16], which were obtained for LSCO at $p = 0.24$. In this case, $A(p = 0.24) = 0.087$, $1/\tau = 500\,\mathrm{K}$, and $\gamma_0 = 1$. Figure 1b shows the temperature dependence of γ for three selected doping values.

The second term in Equation (2) dominates the spectral density above a characteristic energy ω_p, cf. Figure 1. Since ω_p is temperature independent, this contribution generally does not obey MFL scaling except in the high-frequency regime $\omega \gg \omega_p$.

An important remark is in order now to make a comparison between SFL and MFL based on the specific forms of the interaction mediators. A MFL corresponds to a mediator spectral density of the form sketched in Figure 2(a). In this case the phenomenologically assumed broad spectral weight is either constant or linear in ω/T, thereby displaying a full scaling in this variable. On the other hand, the SFL interaction mediator, as already described above, is sketched in Figure 2(b). In this latter case, none of the two contributions is scaling in ω/T: The flattish 'paramagnon' contribution because it does depend on frequency, but not on temperature, while the CDF peak has a temperature dependent slope at low frequency, but it also contain a scale $M/\gamma(T)$, which only becomes small in specific conditions (low T, suppression of superconductivity, finite doping range) when $\gamma(T)$ becomes large. Nevertheless, the sum of these two contributions conspire to mimic a MFL mediator spectral density, with a (nearly) constant flat part at large frequencies and a low energy part linear in ω with a slope that increases when M/γ decreases.

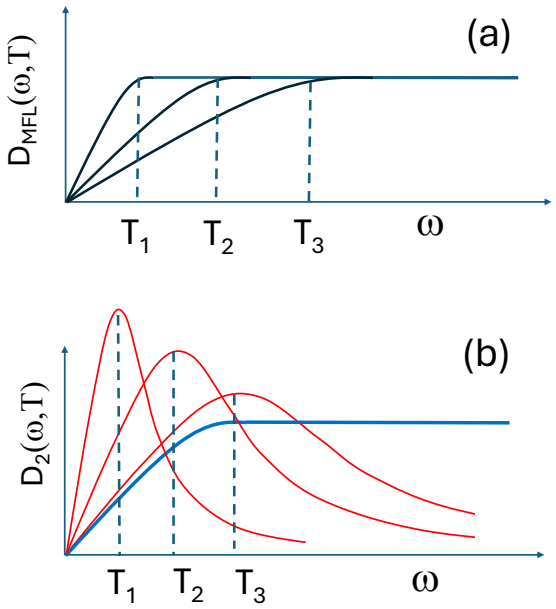

Figure 2. Sketch of the spectral density of the interaction mediators in (a) MFL and (b) SFL models.

Then it is not so surprising that SFL rather closely mimics the MFL, although no true ω/T scaling is formally present in it. This finding is also supported by previous theoretical calculations [43], where it was shown that a MFL optical conductivity might well be due to broad overdamped paramagnons of the form of Equation (2), showing that similar MFL optical behaviors can arise from somewhat different (but broad) excitation spectra.

2.2. Optical Conductivity Calculation

In the case of local interactions, vertex corrections are perturbatively small in the calculation of optical conductivity. Therefore it is customary to use the Allen approximation approach [44], where only the electron self-energy enters the calculation. Although vertex corrections might instead be present in the perturbative expansion of the self-energy, owing to the small-moderate value of

 doi:10.20944/preprints202410.1519.v1

the coupling between quasiparticles and CDF [9] and phonons, we here assume that the one-loop approximation is sufficient. Then we obtain the imaginary part of the one-loop electron self-energy as

$$\Sigma_2(\omega) = -g^2 N(0) \int \mathrm{d}\omega' D_2(\omega' - \omega)\big[f(\omega') + b(\omega' - \omega)\big], \tag{4}$$

with $f(\omega)$ and $b(\omega)$ denoting Fermi and Bose function, respectively, and we have assumed a constant electron density of states $N(0)$. As can be seen from Figure 3a, $\Sigma_2(\omega)$ shows a remarkable scaling of $\Sigma_2(\omega/kT)$ above $\omega/kT \sim 20$ although, as stated above, the individual contributions from CDF and paramagnons do not scale. As illustrated in Figure 3b, this is due to a subtle cancellation between the CDF and paramagnon self-energy shifts, which holds as long as both have comparable spectral density and the coupling of charge carriers $g^2N(0)$ to both excitations is the same. It should be noted that the approximate ratio of 2 between the intensities of low-energy CDF and higher energy fluctuations in our model spectrum Figure 1 is also compatible with the RIXS spectrum in Figure 1c of Ref. [8]. Therefore, our choice of parameters which supports the cancellation between CDF and paramagnon self-energy shifts is mirrored in the experiment.

Since the self-energy is momentum independent one can, after performing a Kramers-Kronig transformation for the real part $\Sigma_1(\omega)$, evaluate the optical conductivity within the Allen approach [44]

$$\sigma(\omega + \mathrm{i}\eta) = \frac{\mathrm{i}\kappa}{\omega} \int \mathrm{d}\omega' \frac{f(\omega') - f(\omega' + \omega)}{\omega - \Sigma(\omega' + \omega + \mathrm{i}\eta) + \Sigma^*(\omega' + \mathrm{i}\eta)}\,. \tag{5}$$

For a layered metal, like cuprates, $\kappa = e^2 t/(\hbar d)$, where t is related to the kinetic energy and d is the interlayer spacing. If in Equation (5) ω is measured in eV, then $\kappa = \mathcal{O}(1)[\mathrm{eV}/(\mathrm{k}\Omega \cdot \mathrm{cm})]$.

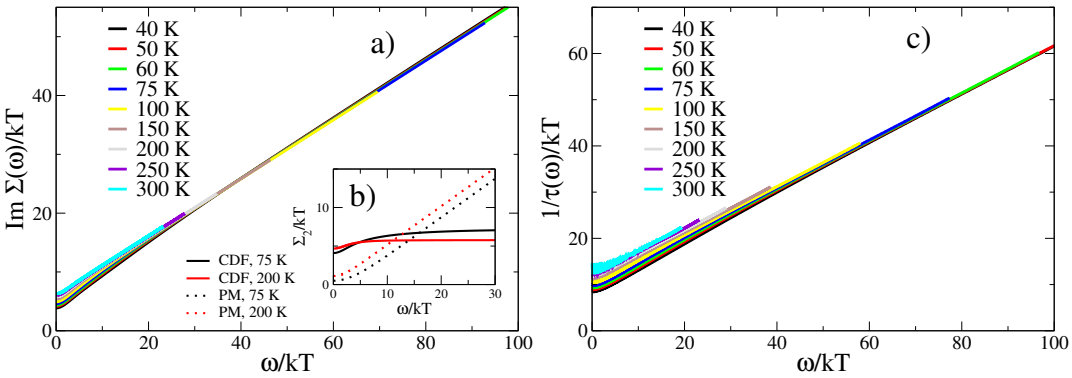

Figure 3. Scaling of the imaginary part of the self-energy (a) and of the optical scattering rate (c). Panel (b) shows the individual contributions to $\Sigma_2(\omega)$ arising from CDF and the higher-energy, mainly paramagnetic (PM), fluctuations. Parameters: $g^2N(0)/\bar{\Omega} = 1.0$, $\bar{\Omega} = 30\,\mathrm{meV}$, $\alpha = 1$, $\omega_p/\bar{\Omega} = 1$, $m/\bar{\Omega} = 0.6$, $\kappa = 1\,\mathrm{eV}/(\mathrm{k}\Omega{\cdot}\mathrm{cm})$.

For an isotropic FL it has been shown [45] that Equation (5) can be represented in terms of a memory function $\mathcal{M}(\omega)$ as [46–48]

$$\sigma(\omega) = \frac{\mathrm{i}\kappa}{\omega + \mathcal{M}(\omega)} = \frac{\kappa}{\frac{1}{\tau(\omega)} - \mathrm{i}\omega\frac{m^*(\omega)}{m_0}}\,. \tag{6}$$

From Equation (6), the optical relaxation time $\tau(\omega)$ and optical mass enhancement $m^*(\omega)/m_0$ are then obtained as

$$\begin{aligned} \frac{1}{\tau(\omega)} &= \kappa\,\mathrm{Re}\left[\frac{1}{\sigma(\omega)}\right], \\ \frac{m^*(\omega)}{m_0} &= -\kappa\,\mathrm{Im}\left[\frac{1}{\omega\sigma(\omega)}\right], \end{aligned}$$

 doi:10.20944/preprints202410.1519.v1

when $\sigma(\omega)$ is evaluated from Equation (5). The optical relaxation time is shown in the lower panel of Figure 3 and displays a scaling behavior similar to that of the self-energy. In fact, in the limit $\omega/kT \gg 1$ one can replace the Fermi functions in Equation (5) by their zero-temperature limit which yields the approximate result [16]

$$\sigma(\omega) = \frac{i\kappa}{\omega - 2\Sigma(\omega/2)},$$

and therefore $1/\tau(\omega) = 2\Sigma_2(\omega/2)$. It is also interesting to observe that below $\omega/kT \approx 20$ the scaling relation in Figure 3c is violated with decreasing temperature. This is exactly the behavior observed in the experimental data (Figure 5c of Ref. [16]) and corresponds to the crossover to a FL, below a temperature scale M/γ within our SFL scenario.

Finally, Figure 4 shows the effective mass correction as a function of frequency for different temperatures. Following Ref. [16], we extract the mass correction at $\omega = 5\,kT$ from the results and plot it as a function of temperature in the inset to Figure 4 (black circles). Moreover, we extract the mass correction at 10 meV and extrapolate it to $\omega = 0.1$ meV, which is shown by the red squares in the inset. Both higher-energy extrapolations of the mass correction show scaling behavior analogous to what is obtained in the experimental data of Ref. [16]. However, the low-energy mass renormalization

$$\frac{1}{Z} = 1 - \left.\frac{\partial\Sigma_1}{\partial\omega}\right|_{\omega=0},$$

represented by the blue dashed line, converges to a constant in the limit $T \to 0$, in agreement with the fact that at the end of the day in this regime we are dealing with a FL [12].

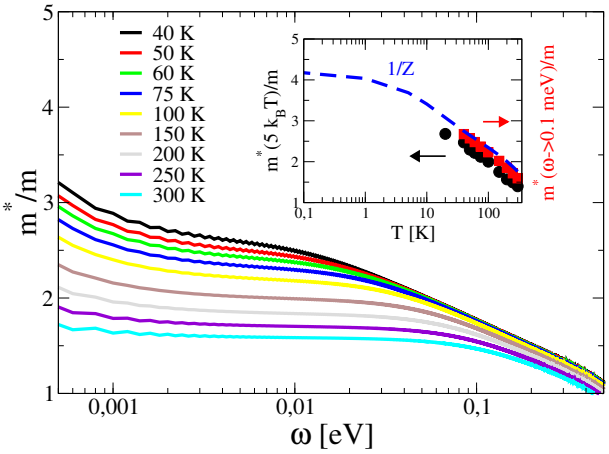

Figure 4. Main panel: Optical mass $m^*(\omega)/m \sim \mathrm{Re}[1/(\omega\sigma(\omega))]$, as extracted from the calculated optical conductivity. The inset shows the values as extracted at $5\,kT$ (black), extrapolated to zero frequency from the plateau at 10 meV (red), and the self-energy mass renormalization $1/Z$ (blue). Parameters: $g^2N(0)/\bar{\Omega} = 0.6$, $\bar{\Omega} = 30$ meV, $\alpha = 1$, $\omega_p/\bar{\Omega} = 1$, $m/\bar{\Omega} = 0.5$, $\gamma = 1$.

3. Discussion and Conclusions

Some general considerations are in order about the optical conductivity analysis carried out here. First of all, the definition of an optical conductivity requires that the electron system has some current dissipation mechanism, otherwise the total momentum conservation would force an identically vanishing conductivity. This is an important issue for those theories that involve the coupling to small momentum order parameter fluctuation (e.g., nematicity). In our case, instead, the SFL scenario involves large momentum scattering, so that umklapp processes are automatically included. Therefore, even disregarding the rich complications of umklapp processes [49], we can safely claim that our CDF mediated scattering does allow for current dissipation, and quenched disorder can be naturally

 doi:10.20944/preprints202410.1519.v1

present, but it is not a crucial ingredient. We also notice that a further current dissipation mechanism is provided by the composite (electronic and phononic) nature of CDF. It was shown long ago [40] that Ward identities, implementing current conservation in a Galilean-invariant system of electrons coupled to purely electronic CDW, are instead violated as soon as the CDW acquire a phononic component, thereby indicating that lattice dynamics can provide an additional current dissipation channel for the electronic subsystem.

The above analysis demonstrates that the experimentally observed RIXS spectrum [8], comprising low-energy CDF plus higher-energy contributions from phonons, particle-hole and paramagnon excitations, contains the needed boson fluctuations to account for the optical properties of cuprates. Moreover, the (approximate) scaling properties identified in optical experiments are well reproduced by our model, although it ultimately describes a FL below an energy (temperature) scale M/γ. The enhancement of the specific heat coefficient in cuprates at very low temperature [20], $T \lesssim 10$ K, forces our model [10] to invoke a shrinking of this energy scale trough a growth of $\gamma(T)$ from 1 to about 5-10 when T is lowered from 20 to 0.5 K. Notice that this substantial increase of γ is only relevant at low temperatures *and in the presence of very strong magnetic fields*, when the superconducting gap is suppressed allowing for a sufficient growth of the electronic damping of the CDF. This is the peculiar SFL effect extending the strange metal T-linear resistivity and the logarithmic specific heat at low T. On the other hand, the optical experiments discussed here [16] are carried out at higher temperatures $T > T_c \sim 40$ K, where the logarithmic increase of the damping plays a minor role and γ increases weakly (by a factor two or so). Therefore the FL energy scale M/γ stays non negligible and leads to the observed violations of the scaling. Of course also elastic scattering from quenched impurities contributes as well making it difficult to use the optical experiment to estimate the M/γ scale and discriminate it from elastic scattering. To do so one should work in the unachievable regime (low T and very large magnetic fields), where γ grows substantially. In practice for the present experiments, the increase of γ is not influential, as we show in Appendix A, where we carry out the same analysis finding good agreement with the data also when $\gamma = 1$. In fact, as shown in the Appendix A, an equivalent description of the optical data from Ref. [16] can be obtained *without* invoking Equation (3) and by fixing the damping parameter to a temperature independent value $\gamma = 1$ (which of course would be at odds with the explanation of specific heat data or linear-in-temperature resistivity down to low temperature). In any case, it is interesting to observe that the violation of the MFL paradigm is observed in the scaling of the optical scattering rate below $\omega/kT \approx 20$ (cf. Figure 3), which is therefore fully compatible with the crossover to a FL, as predicted by our theory. Of course, it may well be that the cuprates are in a genuine MFL state and that the mild scaling violations observed in experiments are due to elastic impurity scattering, the scaling being an intrinsic property. However, one should keep in mind that the scattering in a MFL approaches the unitary limit upon reducing temperature [50]. This should increase $1/\tau(\omega)$, whereas within our theory (and in the experiment) a reduction of $1/\tau(\omega)$ for small T (with respect to the linear relation) is found.

According to our analysis, one should be aware that the simpler explanation of a (Shrinking) FL with low-energy (of $6-8$ meV) CDF plus phonons, particle-hole excitations,and paramagnons is enough to reproduce the data, without assuming any intrinsic scaling property. Of course the proximity to the charge-ordering QCP plays a role in producing abundant CDF which display some quantum critical behavior at short length and time scales.

In conclusion, the present analysis shows that MFL and SFL are both internally consistent pictures calling for further theoretical and experimental investigations to discriminate between them. Comparison with other strange metals like $CeCu_{6-x}(Au,Ag)_x$, pnictides, twisted bilayer graphene and so on might also provide hints.

As far as the violations to the scaling of low-frequency optical spectra is concerned, we wish to add here a final remark. One should be warned that scaling properties of optical spectra should be discussed with caution [40], because many processes can affect the low-frequency optical response of bad metals, partially masking or modifying the contributions arising from self-energy corrections dressing

 doi:10.20944/preprints202410.1519.v1

the charge carriers, that were discussed in this piece of work. The possibility exists that collective excitations may directly contribute to the optical response [51], their coupling to the electromagnetic field being possibly mediated by charge carriers [52]. The contribution to the optical response of processes with CDF alone as intermediate (virtual) states is currently under investigation. Increasing theoretical evidence indicates that slow/overdamped collective excitations can introduce displaced (finite-frequency) peaks in the optical response of bad metals [51,53–55]. Unless an experiment can access the very low-frequency regime, the shoulders of these displaced peaks can be easily mistaken for anomalously large Drude peaks.

Funding: S.C. and M.G. acknowledge financial support from the Italian Ministero dell'Università e della Ricerca, through the PNRR project PE0000023-NQSTI, and specifically the project Topological Phases of Matter, Superconductivity, and Heterostructuresâ Partenariato Esteso 4-Spoke 5 (n. PE4221852A63A88D), and from the Ateneo Research Projects of the University of Rome Sapienza: Competing phases and non-equilibrium phenomena in low-dimensional systems with microscopic disorder and nanoscale inhomogeneities (n. RM12117A4A7FD11B), Models and theories from anomalous diffusion to strange-metal behavior (n. RM12218162CF9D05), Non-conventional aspects for transport phenomena and non-equilibrium statistical mechanics (n. RM123188E830D258). G.S. acknowledges financial support by the Deutsche Forschungsgemeinschaft under SE 806/20-1.

Conflicts of Interest: The authors declare no conflicts of interest.

Appendix A. Results for Constant $\gamma = 1$

As discussed in Section 3, the optical data from Ref. [16] are obtained in a frequency and temperature regime where the logarithmic corrections to the damping factor are negligible. Therefore, we report in this Appendix the results for a fixed $\gamma = 1$, starting again from a propagator which is shown in Figure A1 and, in contrast to Figure 1, does not depend on temperature.

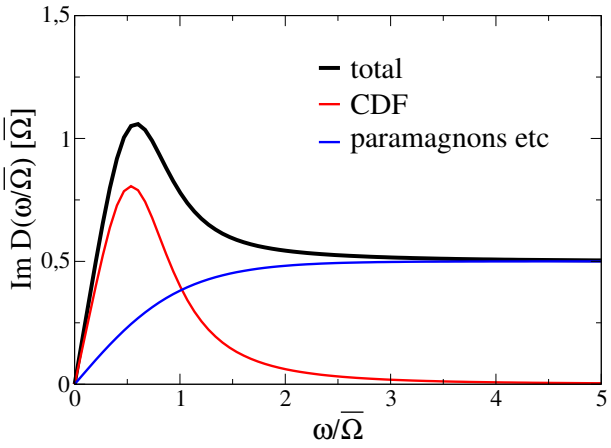

Figure A1. The total spectral density [black, Equation (2)] is composed of the CDF (red) and an effective higher energy contribution (blue) which encompasses phonon, particle-hole and paramagnon excitations Parameters: $\alpha = 1$, $\omega_p/\bar{\Omega} = 1$, $m/\bar{\Omega} = 0.5$, $\gamma = 1$ (see text).

In this case, the temperature dependence is solely given by the Fermi and Bose functions which enter the evaluation of the self-energy Equation (4) and the optical conductivity Equation (5). The resulting scaling behavior of $Im\,\Sigma(\omega)$ and $1/\tau(\omega)$ is shown in Figure A2 and can be compared to the result of Figure 3 obtained within the SFL scenario. Small differences can be observed at low energies, related to the deviation from FL behavior. However, these are far beyond the present experimental accuracy.

 doi:10.20944/preprints202410.1519.v1

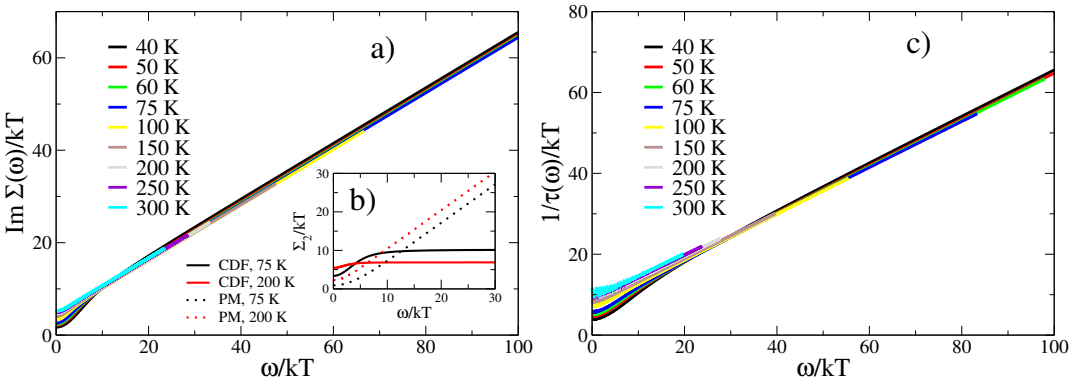

Figure A2. Scaling of the imaginary part of the self-energy (a) and of the optical scattering rate (c). Panel (b) shows the individual contributions to $\Sigma_2(\omega)$ arising from CDF and the higher energy, mainly paramagnetic (PM), fluctuations. Parameters: $g^2N(0)/\bar{\Omega} = 0.6$, $\bar{\Omega} = 30\,\mathrm{meV}$, $\alpha = 1$, $\omega_p/\bar{\Omega} = 1$, $m/\bar{\Omega} = 0.5$, $\kappa = 1\,\mathrm{eV/(k\Omega{\cdot}cm)}$, $\gamma = 1$.

Finally, Figure A2 reports the mass renormalization for the scenario with fixed $\gamma = 1$ which again is close to Figure 4, in particular one observes the crossover to a FL at low temperatures in both cases.

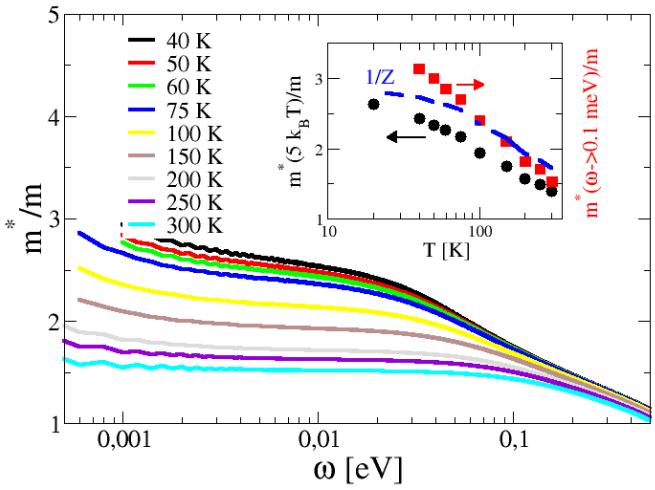

Figure A3. Main panel: Optical mass $m^*(\omega)/m \sim \mathrm{Re}[1/(\omega\sigma(\omega))]$, as extracted from the calculated optical conductivity. The inset shows the values as extracted at $5kT$ (black), extrapolated to zero frequency from the plateau at 10 meV (red), and the self-energy mass renormalization $1/Z$ (blue). Parameters: $g^2N(0)/\bar{\Omega} = 0.6$, $\bar{\Omega} = 30\,\mathrm{meV}$, $\alpha = 1$, $\omega_p/\bar{\Omega} = 1$, $m/\bar{\Omega} = 0.5$, $\gamma = 1$.

References

1. R. L. Greene. The strange metal state of the high-Tc cuprates. Physica C **2023**, 612, 1354319.
2. N. E. Hussey, C. Duffy. Strange metallicity and high-Tc superconductivity: Quantifying the paradigm. Sci. Bull. **2022**, 67, 985-987.
3. S. Sachdev. Strange Metals and Black Holes: Insights From the Sachdev-Ye-Kitaev Model. Oxford Research Encyclopedia of Physics **2023**, https://doi.org/10.1093/acrefore/9780190871994.013.48.
4. A. A. Patel; H. Guo; I. Esterlis; S. Sachdev. Universal theory of strange metals from spatially random interactions. Science **2023**, 381, 790.
5. A. A. Patel; J. McGreevy; D. P. Arovas; S. Sachdev. Magnetotransport in a model of a disordered strange metal. Phys. Rev. X **2018**, 8, 021049.

 doi:10.20944/preprints202410.1519.v1

6. E. Tulipman; N. Bashan; J. Schmalian; E. Berg. Solvable models of two-level systems coupled to itinerant electrons: Robust non-Fermi liquid and quantum critical pairing. arXiv:2404.06532
7. R. Arpaia; S. Caprara; R. Fumagalli; G. De Vecchi; Y. Y. Peng; E. Anderson; D. Betto; G. M. De Luca; N. B. Brookes; F. Lombardi; M. Salluzzo; L. Braicovich; C. Di Castro; M. Grilli; G. Ghiringhelli. Dynamical charge density fluctuations pervading the phase diagram of a Cu-based high-Tc superconductor, Science **2019**, 365, 906-910.
8. R. Arpaia; L. Martinelli; M. M. Sala, S. Caprara; A. Nag; N. B. Brookes; P. Camisa; Q. Li; Q. Gao; X. Zhou; M. Garcia-Fernandez; K.-J. Zhou; E. Schierle; T. Bauch; Y. Y. Peng; C. Di Castro; M. Grilli; F. Lombardi; L. Braicovich; G. Ghiringhelli. Signature of quantum criticality in cuprates by charge density fluctuations. Nat Commun **2023**, 14, 7198. https://doi.org/10.1038/s41467-023-42961-5.
9. G. Seibold; R. Arpaia; Y. Y. Peng; R. Fumagalli; L. Braicovich; C. Di Castro; M. Grilli; G. Ghiringhelli; S. Caprara. Strange metal behaviour from charge density fluctuations in cuprates. Commun. Phys. **2021**, 4, 7.
10. S. Caprara; C. Di Castro; G. Mirarchi; G. Seibold; M. Grilli. Dissipation-driven strange metal behavior. Commun. Phys. **2022**, 5, 1-7.
11. M. Grilli; C Di Castro; G. Mirarchi; G. Seibold; S. Caprara. Dissipative Quantum Criticality as a Source of Strange Metal Behavior. Symmetry **2023**, 15, 569.
12. G. Mirarchi; M. Grilli; G. Seibold; S. Caprara. The Shrinking Fermi Liquid Scenario for Strange-Metal Behavior from Overdamped Optical Phonons. Condensed Matter **2024**, 9, 14.
13. D. van der Marel; H. J. A. Molegraaf; J. Zaanen; Z. Nussinov; F. Carbone; A. Damascelli; H. Eisaki; M. Greven; P. H. Kes; M. Li. Quantum critical behaviour in a high-T_c superconductor. Nature **2003**, 425, 271.
14. D. van der Marel; F. Carbone; A.B. Kuzmenko; E. Giannini. Scaling properties of the optical conductivity of Bi-based cuprates. Annals of Physics **2006**, 321, 1716.
15. E. v. Heumen; X. Feng; S. Cassanelli; L. Neubrand; L. de Jager; M. Berben; Y. Huang; T. Kondo; T. Takeuchi; J. Zaanen. Strange metal electrodynamics across the phase diagram of $Bi_{2-x}Pb_xSr_{2-y}La_yCuO_{6+\delta}$ cuprates. Phys. Rev. B **2022**, 106, 054515.
16. B. Michon; C. Berthod; C. W. Rischau; A. Ataei; L. Chen; S. Komiya; S. Ono; L. Taillefer; D. van der Marel; A. Georges. Reconciling scaling of the optical conductivity of cuprate superconductors with Planckian resistivity and specific heat. Nature Communications **2023** 14:3033.
17. A. El Azrak; R. Nahoum; N. Bontemps; M. Guilloux-Viry; C. Thivet; A. Perrin; S. Labdi; Z. Z. Li; H. Raffy. Infrared properties of $YBa_2Cu_3O_7$ and $Bi_2Sr_2Ca_{n-1}Cu_nO_{2n+4}$ thin films. Phys. Rev. B **1994**, 49, 9846.
18. J. Hwang; T. Timusk; G. D. Gu. Doping dependent optical properties of $Bi_2Sr_2CaCu_2O_{8+\delta}$. J. Phys.: Condens. Mat. **2007**, 19, 125208.
19. C. M. Varma; P. B. Littlewood; S. Schmitt-Rink; E. Abrahams; A. E. Ruckenstein. Phenomenology of the normal state of Cu-O high-temperature superconductors. Phys. Rev. Lett. **1989**, 63, 1996.
20. C. Girod; D. LeBoeuf; A. Demuer; G. Seyfarth; S. Imajo; K. Kindo; Y. Kohama; M. Lizaire; A. Legros; A. Gourgout; H. Takagi; T. Kurosawa; M. Oda; N. Momono; J. Chang; S. Ono; G.-Q. Zheng; C. Marcenat; L. Taillefer; T. Klein. Normal state specific heat in the cuprate superconductors $La_{2-x}Sr_xCuO_4$ and $Bi_{2+y}Sr_{2-x-y}La_xCuO_{6+\delta}$ near the critical point of the pseudogap phase. Phys. Rev. B **2021**, 103, 214506.
21. G. Ghiringhelli; M. Le Tacon; M. Minola; S. Blanco-Canosa; C. Mazzoli; N. B. Brookes; G. M. De Luca; A. Frano; D. G. Hawthorn; F. He; T. Loew; M. Moretti Sala; D. C. Peets; M. Salluzzo; E. Schierle; R. Sutarto; G. A. Sawatzky; E. Weschke; B. Keimer; L. Braicovich. Long-range incommensurate charge fluctuations in $(Y,Nd)Ba_2Cu_3O_{6+x}$. Science **2012**, 337, 821.
22. J. Chang; E. Blackburn; A. T. Holmes; N. B. Christensen; J. Larsen; J. Mesot; R. Liang; D. A. Bonn; W. N. Hardy; A. Watenphul; M. V. Zimmermann; E. M. Forgan; S. M. Hayden. Direct observation of competition between superconductivity and charge density wave order in $YBa_2Cu_3O_{6.67}$. Nature Phys. **2012**, 8, 871.
23. S. Blanco-Canosa; A. Frano; E. Schierle; J. Porras; T. Loew; M. Minola; M. Bluschke; E. Weschke; B. Keimer; M. Le Tacon. Resonant x-ray scattering study of charge-density wave correlations in $YBa_2Cu_3O_{6+x}$. Phys. Rev. B **2014**, 90, 054513.
24. C. Castellani; C. Di Castro; M. Grilli. Singular quasiparticle scattering in the proximity of charge instabilities. Phys. Rev. Lett. **1995**, 75, 4650.
25. C. Castellani; C. Di Castro; M. Grilli. Non-Fermi-liquid behavior and d-wave superconductivity near the charge-density-wave quantum critical point. Z. Phys. B **1996**, 103, 137.

 doi:10.20944/preprints202410.1519.v1

26. C. Castellani; C. Di Castro; M. Grilli. Stripe formation: A quantum critical point for cuprate superconductors. J. of Phys. and Chem. of Sol. **1998**, 59, 1694.
27. G. Seibold; F. Becca; F. Bucci; C. Castellani; C. Di Castro; M. Grilli. Spectral properties of incommensurate charge-density wave systems. Eur. Phys. J. B **2000**, 13, 87.
28. S. Andergassen; S. Caprara; C. Di Castro; M. Grilli. Anomalous Isotopic Effect Near the Charge-Ordering Quantum Criticality. Phys. Rev. Lett. **2001**, 87, 056401.
29. R. Arpaia; G. Ghiringhelli. Charge Order at High Temperature in Cuprate Superconductors. J. Phys. Soc. Japan **2021**, 90, 111005.
30. C. M. Varma; Z. Nussinov; W. van Saarloss. Singular or non-Fermi liquids. Phys. Rep. **2002**, 361, 267.
31. G. R. Stewart. Non-Fermi-liquid behavior in d- and f -electron metals. Rev. Mod. Phys. **2001**, 73, 797.
32. J. A. N. Bruin; H. Sakai; R. S. Perry; A. P. Mackenzie. Similarity of scattering rates in metals showing T-linear resistivity. Science **2013**, 339, 804.
33. M. Taupin; S. Paschen. Are heavy fermion strange metals Planckian. Crystals **2022**, 12, 251.
34. P. W. Phillips; N. E. Hussey; P. Abbamonte. Stranger than metals, Science **2022**, 377,169.
35. S. Ciuchi; S. Fratini. Strange metal behavior from incoherent carriers scattered by local moments. Phys. Rev. B **2023**, 108, 235173.
36. S. Martin; A. T. Fiory; R. M. Fleming; L. F. Schneemeyer; J. V. Waszczak. Normal-state transport properties of $Bi_{2+x}Sr_{2-y}CuO_{6+\delta}$ crystals. Phys. Rev. B **1990**, 41, 846(R).
37. P. Fournier; P. Mohanty; E. Maiser; S. Darzens; T. Venkatesan; C. J. Lobb; G. Czjzek; R. A. Webb; R. L. Greene. Insulator-Metal Crossover near Optimal Doping in $Pr_{2-x}Ce_xCuO_4$: Anomalous Normal-State Low Temperature Resistivity. Phys. Rev. Lett. **1998**, 81, 4720.
38. R. Daou; N. Doiron-Leyraud; D. LeBoeuf; S. Y. Li; F. Laliberté; O. Cyr-Choinière; Y. J. Jo; L. Balicas; J.-Q. Yan; J.-S. Zhou; J. B. Goodenough; L. Taillefer. Linear temperature dependence of resistivity and change in the Fermi surface at the pseudogap critical point of a high-Tc superconductor. Nature Physics **2009**, 5, 31.
39. R. Hlubina; T. M. Rice. Resistivity as a function of temperature for models with hot spots on the Fermi surface. Phys. Rev. B **1995**, 51, 9253.
40. S. Caprara; M. Grilli; C. Di Castro; T. Enss. Optical conductivity near finite-wavelength quantum criticality. Phys. Rev. B **2007**, 75, 140505(R).
41. A. Legros; S. Benhabib; W. Tabis; F. Laliberté; M. Dion; M. Lizaire; B. Vignolle; D. Vignolles; H. Raffy; Z. Z. Li; P. Auban-Senzier; N. Doiron-Leyraud; P. Fournier; D. Colson; L. Taillefer; C. Proust. Universal T-linear resistivity and Planckian dissipation in overdoped cuprates. Nat. Phys. **2019**, 15, 142.
42. B. Michon; C. Girod; S. Badoux; J. Kacmarcik; Q. Ma; M. Dragomir; H. A. Dabkowska; B. D. Gaulin; J. S. Zhou; S. Pyon; T. Takayama; H. Takagi; S. Verret; N. Doiron-Leyraud; C. Marcenat; L. Taillefer; T. Klein. Thermodynamic signatures of quantum criticality in cuprate superconductors, Nature **2019**, 567, 218-222.
43. M. R. Norman; A. V. Chubukov. High-frequency behavior of the infrared conductivity of cuprates. Phys. Rev. B **2006**, 73, 140501R.
44. P. B. Allen. Electron self-energy and generalized Drude formula for infrared conductivity of metals. Phys. Rev. B **2015**, 92, 054305.
45. P. B. Allen. Electron-Phonon Effects in the Infrared properties of Metals, Phys. Rev. B **1971**, 3, 305.
46. W. Götze; P. Wölfle. Homogeneous dynamical conductivity of simple metals. Phys. Rev. B **1972**, 6, 1226.
47. J. W. Allen; J. C. Mikkelsen. Optical properties of CrSb, MnSb, NiSb, and NiAs. Phys. Rev. B **1977**, 15, 2952.
48. D. N. Basov; R. D. Averitt; D. van derMarel; M. Dressel; K. Haule. Electrodynamics of correlated electron materials. Rev. Mod. Phys. **2011**, 83, 471.
49. H.K. Pala; V.I. Yudson; D.L. Maslov. Resistivity of non-Galilean-invariant Fermi- and non-Fermi liquids. Lithuanian Journal of Physics **2012**, 52, 142-164.
50. G. Kotliar; E. Abrahams; A. E. Ruckenstein; C. M. Varma; P. B. Littlewood; S. Schmitt-Rink. Long-Wavelength Behavior, Impurity Scattering and Magnetic Excitations in a Marginal Fermi Liquid. EPL **1991**, 15, 655.
51. S. Caprara; C. Di Castro; S. Fratini; M. Grilli. Anomalous Optical Absorption in the Normal State of Overdoped Cuprates Near the Charge-Ordering Instability. Phys. Rev. Lett. **2002**, 88, 147001.
52. S. Caprara; C. Di Castro; T. Enss; M. Grilli. Low-energy signatures of charge and spin fluctuations in Raman and optical spectra of the cuprates. Journal of Physics and Chemistry of Solids **2008**, 69, 2155-2159.
53. S. Fratini; S. Ciuchi. Displaced Drude peak and bad metal from the interaction with slow fluctuations. SciPost Phys. **2021**, 11, 039.

 doi:10.20944/preprints202410.1519.v1

54. S. Fratini; K. Driscoll; S. Ciuchi; . Ralko. A quantum theory of the nearly frozen charge glass. SciPost Phys. **2023**, 14, 124.
55. H. Rammal; A. Ralko; S. Ciuchi; S. Fratini. Transient localization from the interaction with quantum bosons. Phys. Rev. Lett. **2024**, 132, 266502.